Spherical-wave AVO modeling in elastic and anelastic media

Arnim B. Haase and Charles P. Ursenbach

ABSTRACT

The AVO-response of two-layer isotropic models for AVO-Classes 1 and 3 is investigated for P-waves and converted waves. Zoeppritz reflection coefficients and the Weyl/ Sommerfeld-integral are utilized for the computations. Spherical wave results for R_{PP} and R_{PS} are compared with plane wave reflectivity. Depth dependence of spherical wave AVO is found to be strongest near critical angles of Class 1. There is some similarity between R_{PP} and R_{PS} for Class 1. Normalized Class 3 responses show no depth dependence. There is no similarity between R_{PP} and R_{PS} for Class 3.

Anelasticity modifies the AVO-response of two-layer isotropic models. When reflection amplitude losses due to attenuation are compensated for by unit reflectivity scaling, AVO-characteristics similar to the elastic situation are found. Q-factor dependence of spherical wave AVO is found to be strongest near critical angles of Class 1. This Q-dependence, to some degree, mimics depth dependence of elastic comparisons. Normalized spherical wave Class 3 responses show a mild Q-factor dependence for the highest attenuation levels modelled at Q_{P1} = 100. Wavelet stretch of converted wave AVO reflection traces is observed in addition to a phase rotation of all anelastic trace examples when compared to the elastic situation.

INTRODUCTION

Amplitude-versus-offset analysis was introduced by Ostrander (1984) and is also mentioned in a paper by Hron et al. (1986) as amplitude versus distance. AVO-analysis and AVO-inversion are now widely accepted tools in seismic exploration. The common approach is plane-wave analysis, and linear approximations of the Zoeppritz equations are utilized to this end. For these approximations small incidence angles and small parameter changes are assumed. In recent years, three-parameter AVO-inversion has been investigated for the extraction of density information (e.g. Downton and Lines, 2001). It was observed that, for reasonably accurate density estimates, larger offsets/angles are required than normally used for two parameter inversion, preferably even postcritical events if present (Downton and Ursenbach, 2006). Linearized approximations begin to break down at larger angles and are not applicable near critical points. Even "exact Zoeppritz" is a plane wave approximation to the real world. Winterstein and Hanten (1985) show that cylindrical wave modeling results in a much better fit of seismic data than does plane wave modeling near critical angles. Instead of the amplitude jump at the critical angle predicted by plane-wave theory, they find a more gradual amplitude transition for cylindrical wave models and actual data. The question arises as to what the spherical wave AVO-response might be. Krail and Brysk (1983) attempted to address this question, but incorporated a number of approximations. This modeling study employs only one minimal approximation (see Theory section) and investigates the spherical wave AVO-response for AVO-Classes 1 and 3.

All rocks encountered in nature are anelastic to some degree. Anelasticity causes atten-

uation and velocity dispersion of seismic waves. Velocity dispersion means velocities are functions of frequency. This frequency dependence of seismic velocities can be quantified by frequency independent quality factors Q (Kjartansson, 1979). Q-factors are useful for amplitude/phase compensation and as lithology indicators, but it is well known that plane wave AVO-responses are also Q-factor dependent (see for example Carcione et al., 1998). What, then, is the spherical wave AVO-response in anelastic situations? This modeling study seeks also to quantify the sensitivity of spherical wave AVO-responses (Class 1 and 3) with respect to finite Q-factors.

THEORY

Spherical-wave reflections in elastic media

Plane-wave particle motion reflection and transmission coefficients for elastic isotropic media in welded contact are given by the Zoeppritz equations. The formalism for expressing spherical wave fronts as contour integrals over plane waves goes back to Weyl (1919). The theory describing the interaction of a spherical wave with a planar interface is well established (see for instance Aki and Richards, 1980). In this section we outline the derivation of expressions appropriate to the solid-solid elastic interface. We begin by considering displacement potentials for monochromatic P- and S-waves above and below the interface.

An incident monochromatic spherical wave has the P-wave displacement potential

$$\phi^{\text{inc}} = \frac{1}{R}\exp\left(i\omega\frac{R}{\alpha_1} - i\omega t\right). \tag{1}$$

where R is the distance from the source, ω is frequency, t is time, and α_1 is the P-wave velocity of the upper layer (in which the source is located.) In Cartesian coordinates this can be written as an integral over plane waves, $\exp[\pm i(k_x x + k_y y + k_z z)]$, subject to the dispersion relation, $k_z = \sqrt{\omega^2/c^2 - k_x^2 - k_y^2}$. Such an expression is called the *Weyl integral*. If the interface is horizontal, and the media are isotropic, or at least are limited to vertical transverse isotropy, then one can assume cylindrical symmetry, and the Weyl integral can be reduced to the *Sommerfeld integral*. This expresses ϕ^{inc} in terms of cylindrical waves, which can be constructed by integrating together all common-azimuth plane waves. Defining $r \equiv \sqrt{x^2+y^2}, \theta \equiv \tan^{-1}(y/x), k_r \equiv \sqrt{k_x^2+k_y^2}$, and $\theta_k \equiv \tan^{-1}(k_y/k_x)$, then

$$\begin{aligned} & \int_0^\infty \exp[\pm i(k_x x + k_y y + k_z z)]d\theta_k \\ = & \int_0^\infty \exp[\pm i(k_r r\cos(\theta_k - \theta) + k_z z)]d\theta_k \\ = & \ 2\pi J_0(k_r r)e^{\pm ik_z z} \end{aligned}$$

These cylindrical waves appear in the Sommerfeld integral which, following Aki and Richards (1980), we write as

$$\phi^{\text{inc}} = Ai\omega\exp(-i\omega t)\int_0^\infty \frac{p}{\xi_1}J_0(\omega p r)\exp(i\omega\xi_1|z|)dp. \tag{2}$$

Here we have transformed from wavenumber to slowness notation, where k_r/ω is the horizontal slowness p, and k_z/ω is the vertical slowness ξ (for P-waves) or η (for SV-waves). The constant A represents the amplitude of the incident wave.

The potentials for reflected and transmitted waves can, by symmetry considerations, also be written in terms of cylindrical waves, but the waves are not necessarily spherical, so an arbitrary p-dependent weighting factor must be included in the integrand, i.e.,

$$\phi^{R_{\rm PP}} = i\omega \exp(-i\omega t) \int_0^\infty B(p) \frac{p}{\xi_1} J_0(\omega p r) \exp(-i\omega \xi_1 z) dp \tag{3}$$

$$\psi^{R_{\rm PS}} = i\omega \exp(-i\omega t) \int_0^\infty C(p) \frac{p}{\xi_1} J_0(\omega p r) \exp(-i\omega \eta_1 z) dp \tag{4}$$

$$\phi^{T_{\rm PP}} = i\omega \exp(-i\omega t) \int_0^\infty D(p) \frac{p}{\xi_1} J_0(\omega p r) \exp(i\omega \xi_2 z) dp \tag{5}$$

$$\psi^{T_{\rm PS}} = i\omega \exp(-i\omega t) \int_0^\infty E(p) \frac{p}{\xi_1} J_0(\omega p r) \exp(i\omega \eta_2 z) dp \tag{6}$$

where ψ represents an S-wave displacement potential. Note that the boundary conditions as $z \to \pm\infty$ dictate the sign of the exponent. In this case we assume that if $k_z^2 < 0$, then k_z will be positive imaginary for positive frequencies and negative imaginary for negative frequencies.

Next we generate equations to solve for $B(p), C(p), D(p)$ and $E(p)$. These are obtained by boundary conditions relating displacement and stress across the interface. The displacement is obtained from the potentials by the relation (Aki and Richards, 1980)

$$\mathbf{u} = \nabla\phi + \nabla \times \nabla \times (0, 0, \psi). \tag{7}$$

Carrying this out in cylindrical coordinates yields the non-zero displacement components u_r and u_z. The stress components which must be continuous across the interface are

$$\tau_{zr} = \mu \left(\frac{\partial u_r}{\partial z} + \frac{\partial u_z}{\partial r} \right), \tag{8}$$

$$\tau_{zz} = \lambda \nabla \cdot \mathbf{u} + 2\mu \frac{\partial u_z}{\partial z}, \tag{9}$$

where λ and μ are the usual Lamé constants. These operations are applied first to $\phi^{\rm inc} + \phi^{{\rm R}_{PP}}$, $\psi^{{\rm R}_{PS}}$ to obtain $u_r^{(1)}, u_z^{(1)}, \tau_{zr}^{(1)}$, and $\tau_{zz}^{(1)}$, then similarly for the lower layer. The reflection and transmission properties are independent of the location of the interface, so it is convenient to define it at $z = 0$. We then set $u_r^{(1)}(z = 0) = u_r^{(2)}(z = 0)$ and similarly for other displacement and stress components. Each of these four equations can be collected into a single integral, the integrand of which must equal zero for each value of p. This yields four algebraic equations linear in A, B, C, D, and E. Comparing the results to those

for plane waves (Aki and Richards, 1980) yields the relations

$$B(p) = Ae^{i\xi_1 h} R_{\text{PP}}^{\text{pw}}(p) \tag{10}$$

$$C(p) = Ae^{i\xi_1 h} \frac{1}{i\omega p} \frac{\beta_1}{\alpha_1} R_{\text{PS}}^{\text{pw}}(p) \tag{11}$$

$$D(p) = Ae^{i\xi_1 h} \frac{\alpha_2}{\alpha_1} T_{\text{PP}}^{\text{pw}}(p) \tag{12}$$

$$E(p) = Ae^{i\xi_1 h} \frac{1}{i\omega p} \frac{\beta_2}{\alpha_1} T_{\text{PS}}^{\text{pw}}(p) \tag{13}$$

where α_i, β_i are the P-wave and S-wave velocities of the i^{th} layer. Substituting these expressions into equations 3 to 6 yields explicit expressions for the displacement potentials of reflected and transmitted waves, and shows that they are given as integrals over the analogous plane-wave reflection and transmission coefficients for the interface.

The final result is that the required potentials may be calculated as

$$\phi^{R_{\text{PP}}} = Ai\omega e^{-i\omega t} \int_0^\infty R_{\text{PP}} \frac{p}{\xi} J_0(\omega p r) e^{i\omega\xi(z+h)} dp \tag{14}$$

$$\psi^{R_{\text{PS}}} = Ai\omega e^{-i\omega t} \int_0^\infty \left(\frac{1}{i\omega p} \frac{\beta}{\alpha} R_{\text{PS}} \right) \frac{p}{\xi} J_0(\omega p r) e^{i\omega(\xi h + \eta z)} dp \tag{15}$$

Reflections from an elastic interface are computed firstly by introducing particle motion reflection coefficients given by the Zoeppritz equations. Secondly, particle motion **u** is computed from equation 7 and from the potentials given by equations 14 and 15. Thirdly, it is assumed that displacement is parallel to the ray direction for PP reflected waves, and perpendicular for PS waves. Other displacement components are neglected. (This is the sole approximation in the procedure and introduces very little error (Ursenbach et al., 2006)). Fourthly, normalization by the maximum particle motion magnitude for unit reflectivity leads to spherical wave PP and PSv reflection coefficients. The integrations shown in equations 14 and 15 proceed one frequency point at a time. When all frequency points are computed for the desired output bandwidth, the time domain response is found by inverse Fourier transform. Quadrature traces are determined by Hilbert transform. From these two trace types amplitude and phase of reflected spherical waves can be calculated

Extension to anelasticity

A mathematical treatment of anelasticity can be found in Aki and Richards (1980). They show that causality requires velocity dispersion and derive the following equation:

$$\nu(\omega) = \nu_{\text{ref}} \left(1 + \frac{\ln(\omega/\omega_{\text{ref}})}{\pi Q} - \frac{i}{2Q} \right), \tag{16}$$

where Q is a frequency independent quality factor. As in the elastic case before, spherical wave displacements **u** are computed from the potentials $\phi^{R_{PP}}$ and $\psi^{R_{PS}}$.

The integrations shown in equations 14 and 15 again proceed one frequency point at a time. However, in the anelastic situation velocities are complex and must be recomputed

for every frequency point, according to equation 16. The P-wave quality factor for the top layer (Q_{P1}) is assumed to be known for the computations and is listed in the figures. Q_{P2} (for the bottom layer) as well as S-wave quality factors Q_{S1} and Q_{S2} are calculated with the aid of empirical equations (Waters, 1978; Udias, 1999).

$$\frac{1}{Q_P} = \left(\frac{\text{const.}}{\alpha}\right)^2, \tag{17}$$

and

$$Q_S = Q_P \frac{4}{3}\left(\frac{\beta}{\alpha}\right)^2. \tag{18}$$

MODELING

An actual gas-sand reservoir from the prairies is utilized to derive two layer models for this study. Density ρ_1 is 2400 kg/m^3 for the layer just above the reservoir. P-wave velocity α_1 = 2000 m/s is dictated by a reservoir depth of 500 m and a corresponding two-way traveltime of approximately 500 ms. The layer parameters for AVO-Classes 1 and 3 shown in Table 1 are adapted from Rutherford and Williams (1989). Output signal bandwidth and linear edge tapers are determined by choosing a 5/15-80/100 Hz Ormsby wavelet as the source signature. Free surface effects are not considered in this study. A P-wave point source and spherical wave fronts are assumed for the computations.

Table 1. Elastic parameters for two-layer models.

Class	α_1/[m/s]	β_1/[m/s]	ρ_1/[kg/m^3]	α_2/[m/s]	β_2/[m/s]	ρ_2/[kg/m^3]
1	2000	879.88	2400	2933.33	1882.29	2000
3	2000	879.88	2400	1963.64	1260.04	2000

Figures 1 and 2 show AVO-response magnitudes computed from trace envelopes. AVO-Class 1 comparisons are given in Figure 1a (for PP-waves) and Figure 1b (for converted waves). Similarly, AVO Class 3 results are shown in Figure 2. Plane wave comparisons are added to all AVO magnitude responses in order to highlight the impact of spherical wave fronts. Figures 3 and 4 display spherical wave PP and PS-reflection *traces* for AVO Classes 1 and 3. These trace displays are scaled individually in order to accommodate maximum amplitudes. Clipping of maximum trace amplitudes is indicated by colour changes.

The same two layer model as was utilized in the elastic situation is also employed in the anelastic study. All velocities listed in Table 1 are taken to be reference velocities here; the reference frequency (see equation 16) is set to 50 Hz. As before, a 5/15-80/100 Ormsby wavelet is chosen as the source signature; a P-wave point source is assumed. Free surface effects are ignored.

Two values are assumed for the top layer P-wave quality-factor: firstly, Q_{P1} = 100 and, secondly, Q_{P1} = 387.5 . The other Q-factors are calculated from equations 17 and 18 and are listed in Table 2.

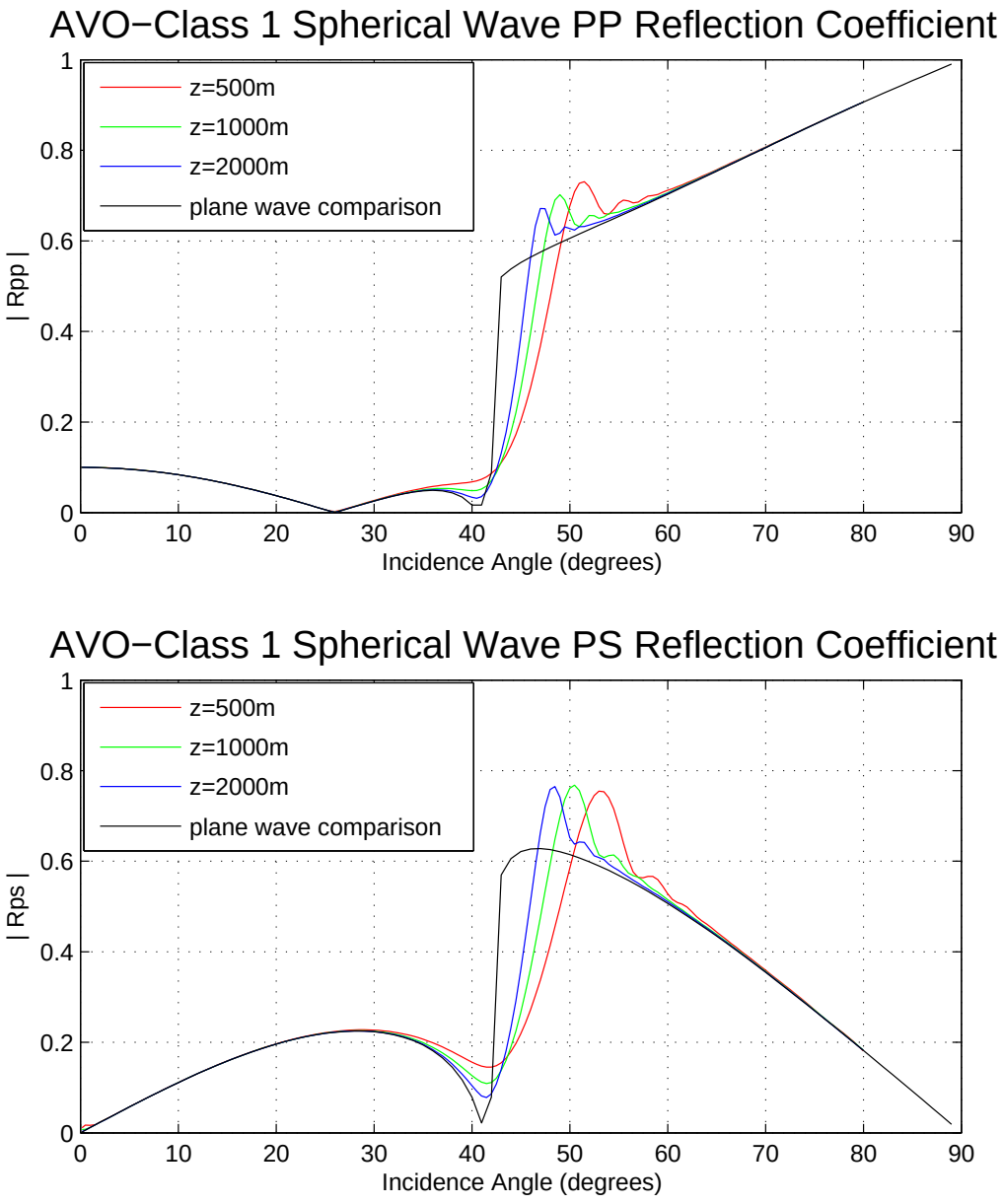

FIG. 1. Spherical-wave reflection coefficients for Class 1 AVO, (a) PP (b) PS.

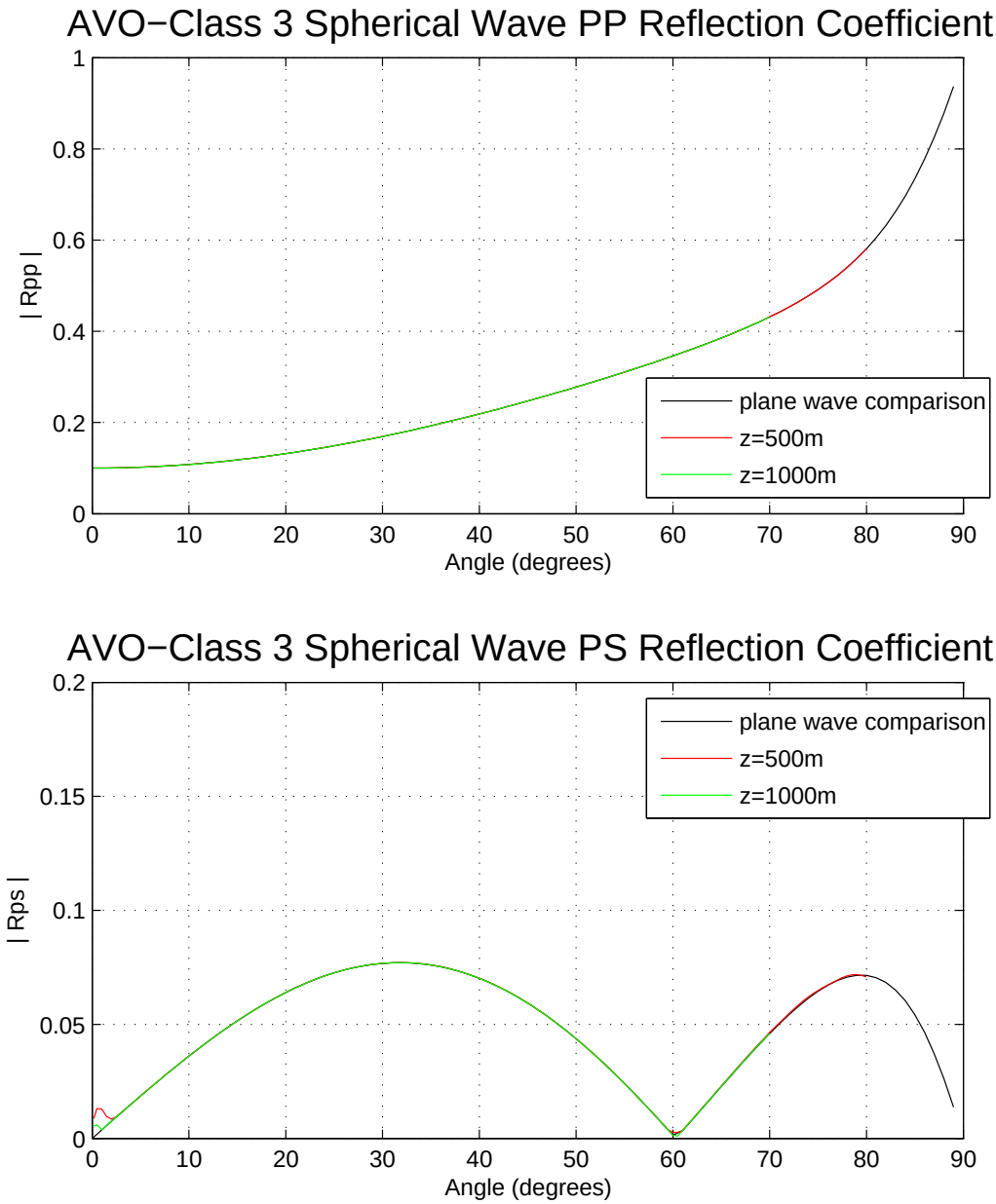

FIG. 2. Spherical-wave reflection coefficients for Class 3 AVO, (a) PP (b) PS.

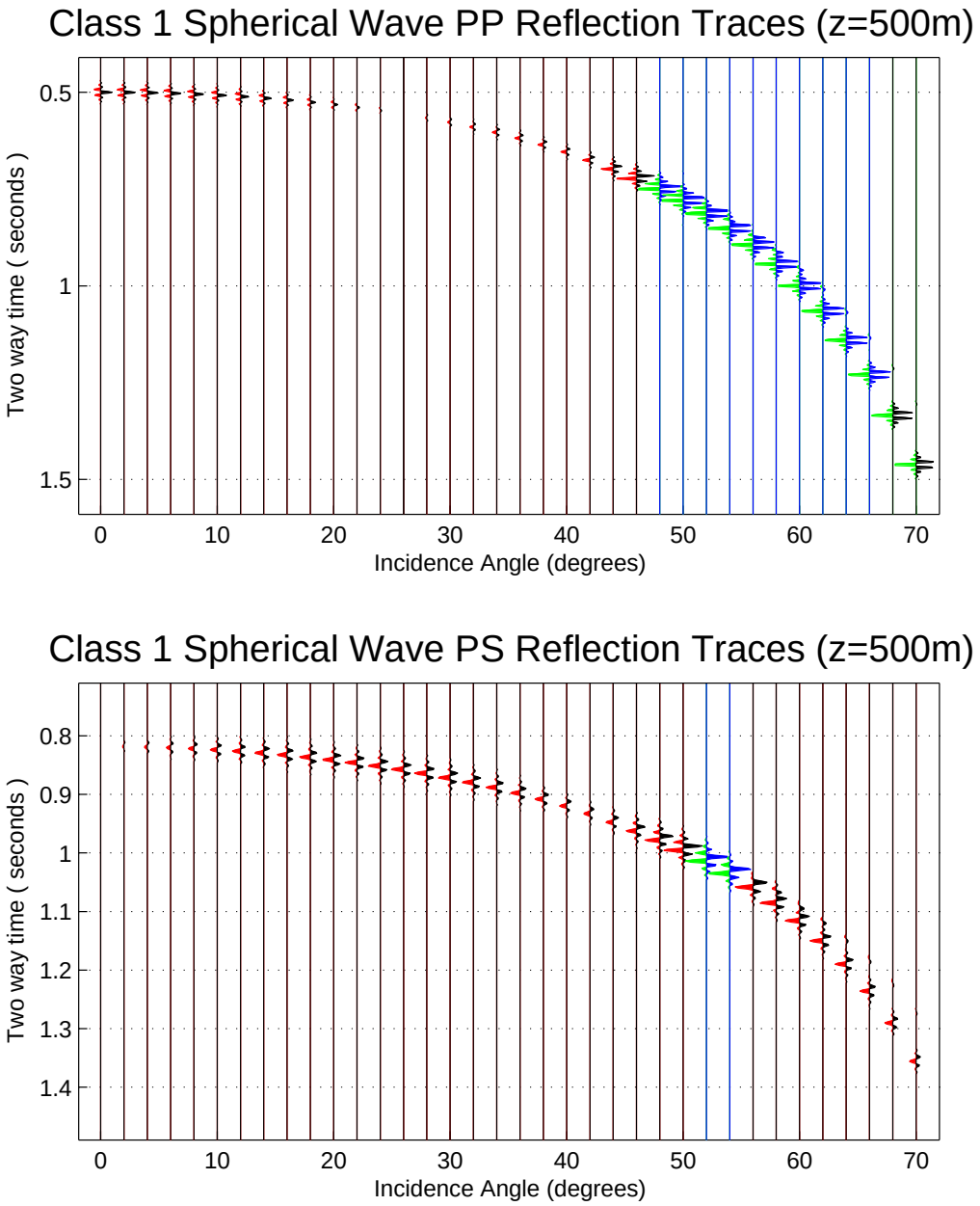

FIG. 3. Spherical-wave reflection traces for Class 1 AVO, (a) PP (b) PS.

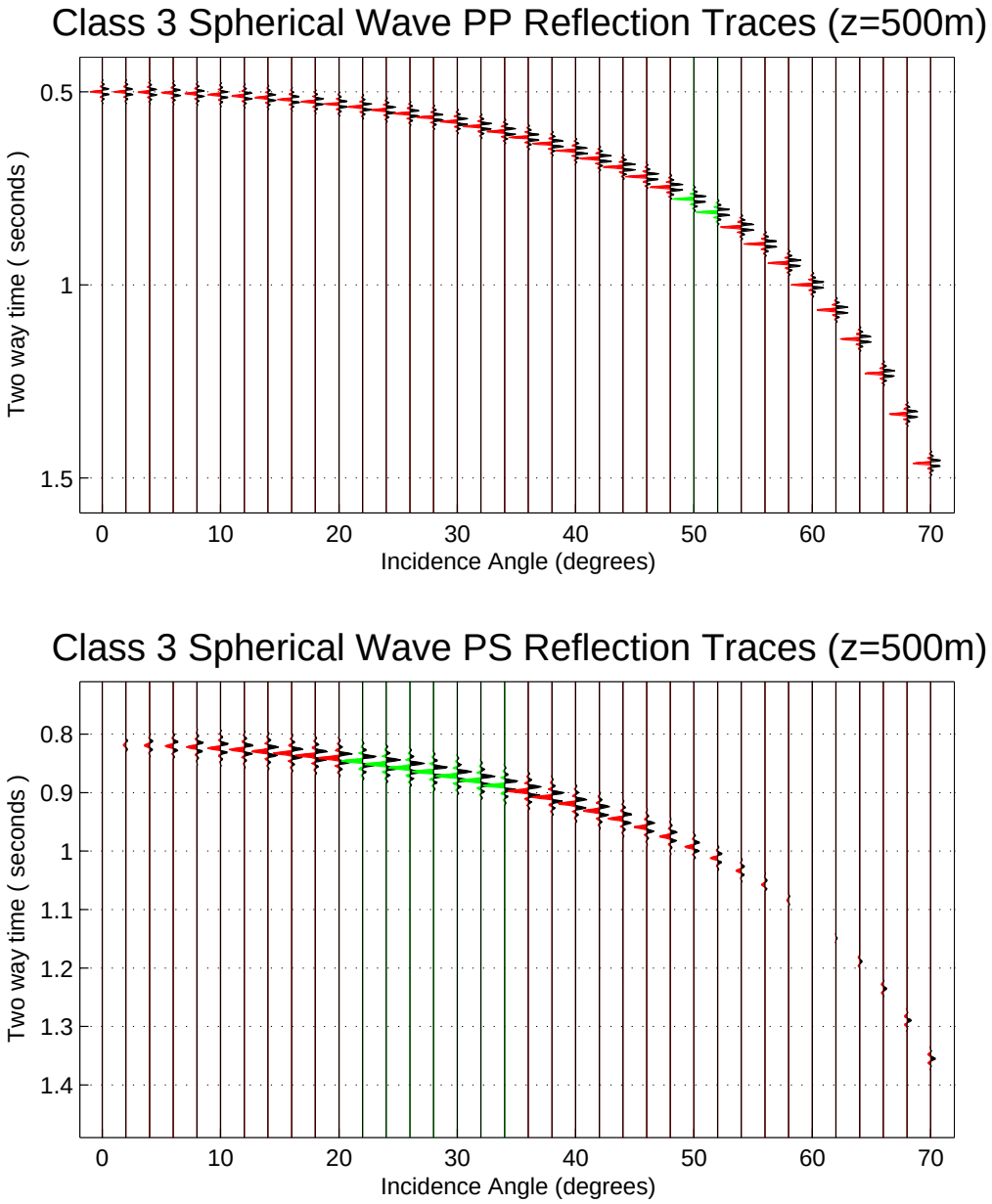

FIG. 4. Spherical-wave reflection traces for Class 3 AVO, (a) PP (b) PS.

Table 2. Q-factors derived from Q_{P1}=100 and 387.5. These represent strongly and weakly attenuating two-layer models.

Class	Q_{P1}	Q_{P2}	Q_{S1}	Q_{S2}
1	100	215.1	25.8	118.1
3	100	96.4	25.8	52.9
1	387.5	833.5	100	457.6
3	387.5	373.5	100	205.1

Figures 5 and 6 show anelastic spherical wave AVO-responses for Classes 1 and 3. Plane-wave and elastic spherical-wave responses are given for comparison. PP- and PS-reflection traces for AVO Classes 1 and 3 of the anelastic case are displayed in Figures 7 and 8.

Scaling of Amplitudes

The appearance of computed AVO results depends on scaling. Spherical spreading must be compensated for if results are to be compared to plane wave responses. Figure 9 shows scaling comparisons for Class 1 PP-AVO. The layer parameters for Class 1 AVO in Table 1 give a plane wave zero offset reflection coefficient of 0.1. Normalizing the zero offset spherical wave response to 0.1 gives good agreement with the plane wave response up to about 30° incidence angle. Spherical spreading can be compensated for by 1/cos-scaling. Applying 1/cos-scaling to the spherical wave response brings it much closer to a plane wave comparison at angles well beyond critical. All normalization factors used to compute Figures 1, 2, 5 and 6 are derived by setting reflection coefficients R in equations 14 and 15 to unity. Inspection of Figures 1a and 9 shows that unity-R scaling provides the highest level of agreement between spherical wave responses and plane wave responses.

The trace displays (Figures 3, 4, 7 and 8) are scaled individually in order to accommodate maximum amplitudes. Clipping of maximum trace amplitudes is indicated by colour changes.

DISCUSSION

For Class 1 AVO-models, P-wave and S-wave velocities are increasing across the interface as can be seen in Table 1. Because of this velocity increase critical angles exist and head waves are generated in Class 1 models. A head wave can be seen separating from reflected waves at the highest angles in Figure 3b. It also exists in Figure 3a, but is not as evident for the angles shown. The PSv-reflection traces in Figure 3b start with zero amplitude at zero angle. Then a negative reflection ($-180°$ of angle) grows stronger towards a magnitude maximum just below 30°. Beyond 30° the PSv-reflection strength diminishes first and then goes through a 90° phase rotation and increasing strength near the critical angle just beyond 40°. With angles increasing beyond that, amplitudes diminish towards zero at 90° and the phase angle returns to $-180°$. Figure 1a shows the magnitude of R_{PP} for Class 1. The greatest departure from a plane wave comparison is observed in the vicinity of the critical angle. The larger the reflector depth, the closer the spherical response to the plane wave comparison; however, even at 2000 m depth, there are significant differences. The Class 1 PSv-reflection comparison in Figure 1b bears striking similarities to its PP counterpart in the way it differs from plane wave behavior near the critical angle. The depth dependence of spherical wave Class 1 AVO-responses of R_{PP} and R_{PS} is quite similar

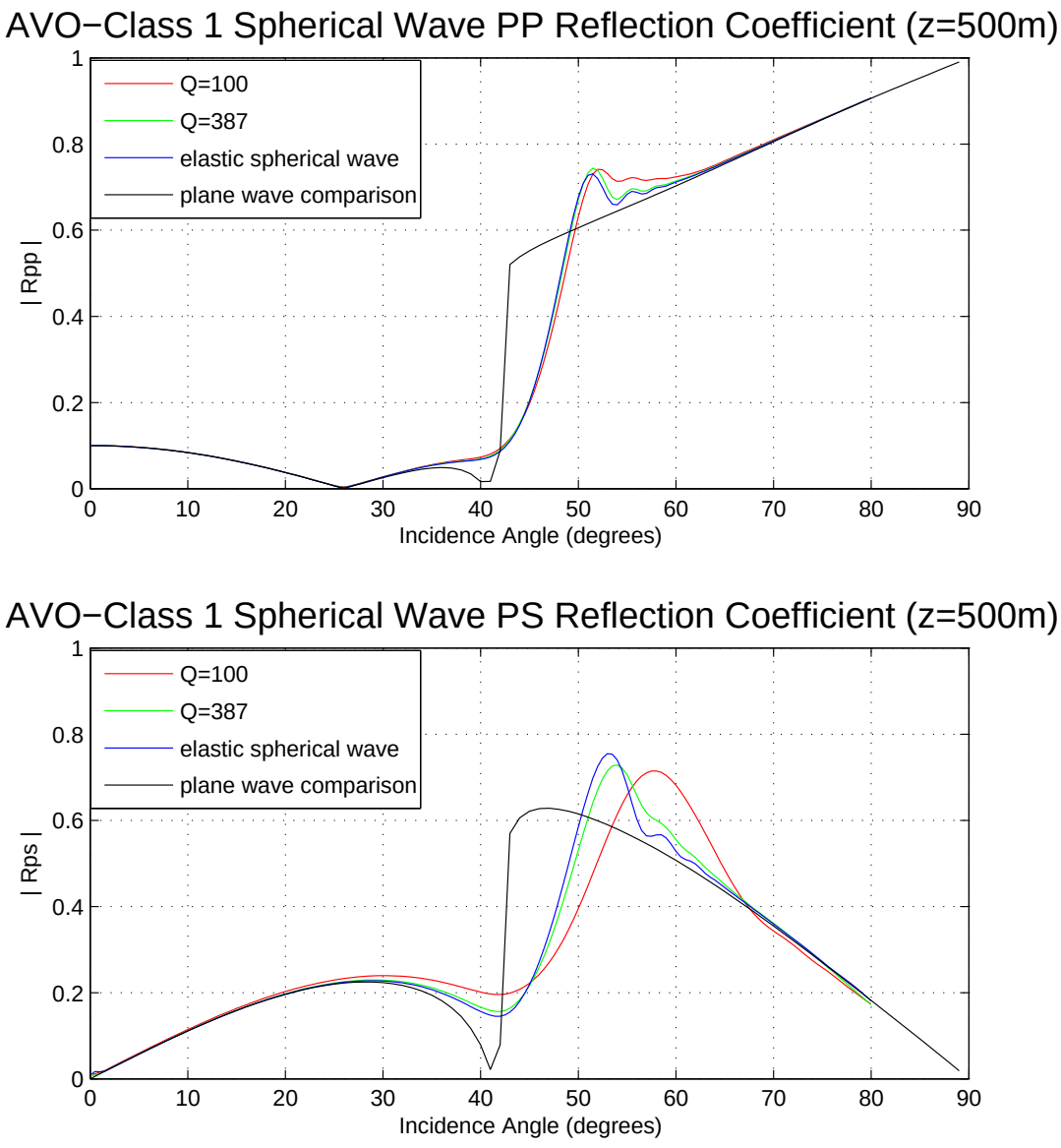

FIG. 5. Anelastic spherical-wave reflection coefficients for Class 1 AVO, (a) PP (b) PS.

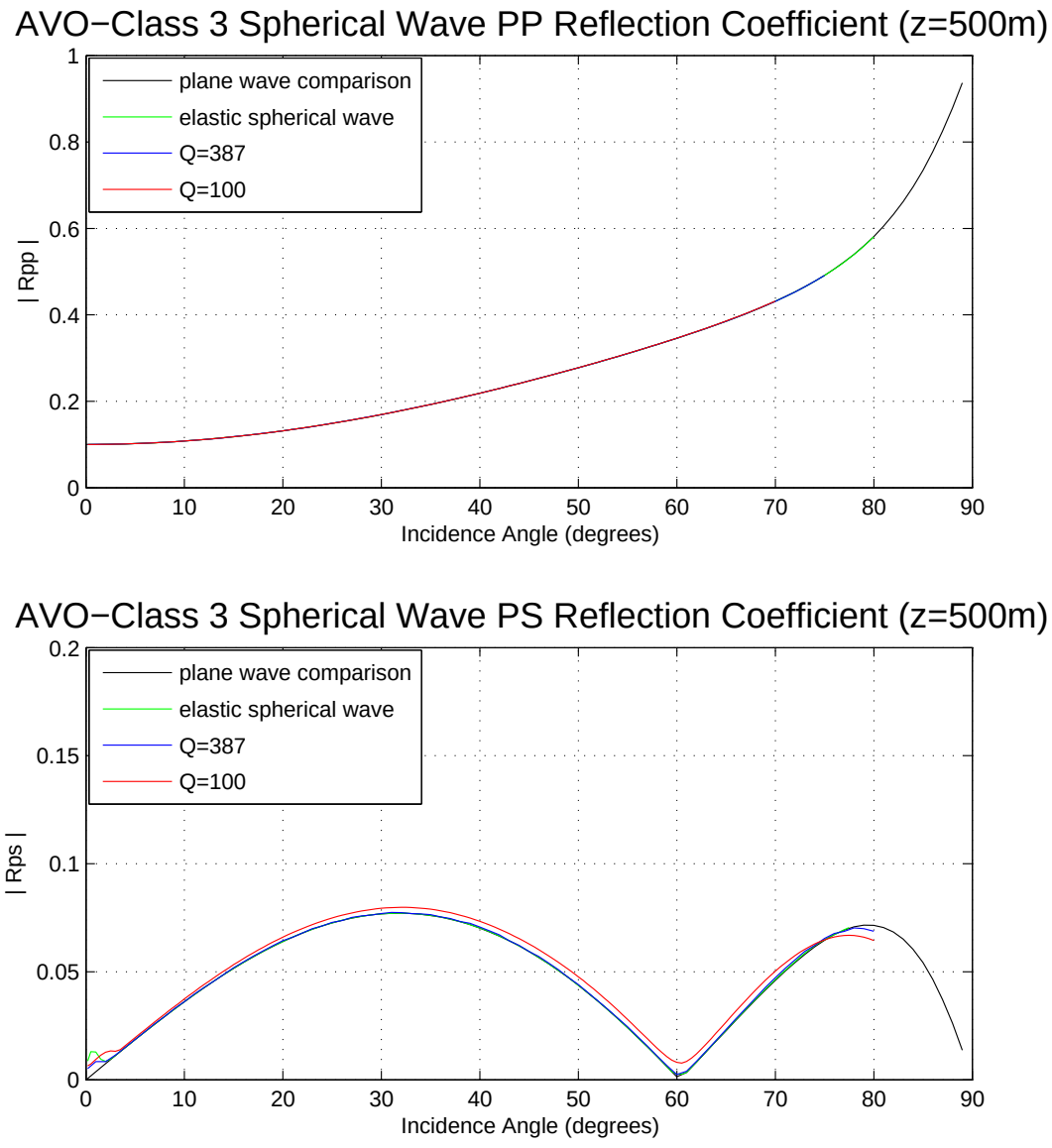

FIG. 6. Anelastic spherical-wave reflection coefficients for Class 3 AVO, (a) PP (b) PS.

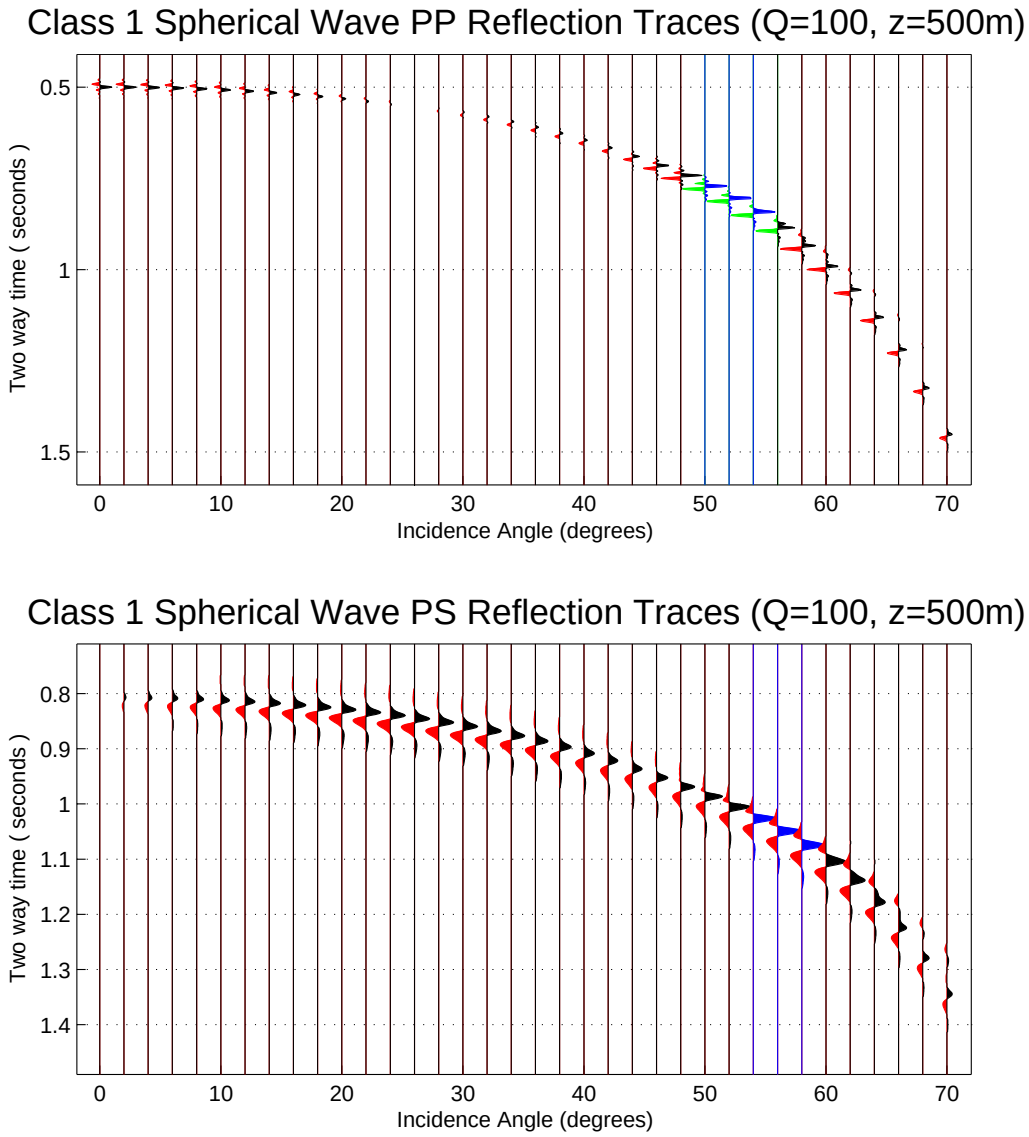

FIG. 7. Anelastic spherical-wave reflection traces for Class 1 AVO, (a) PP (b) PS.

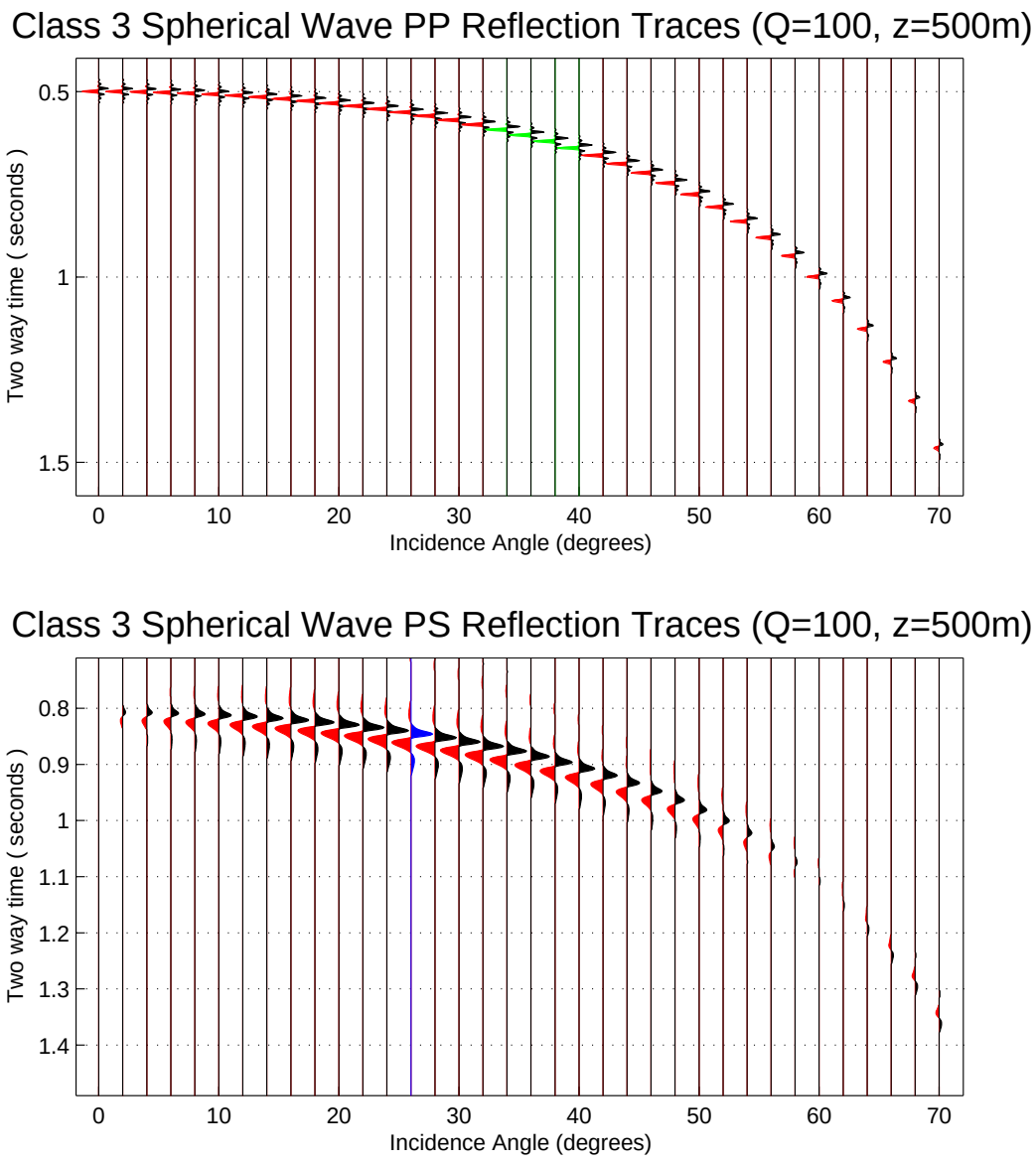

FIG. 8. Anelastic spherical-wave reflection traces for Class 3 AVO, (a) PP (b) PS.

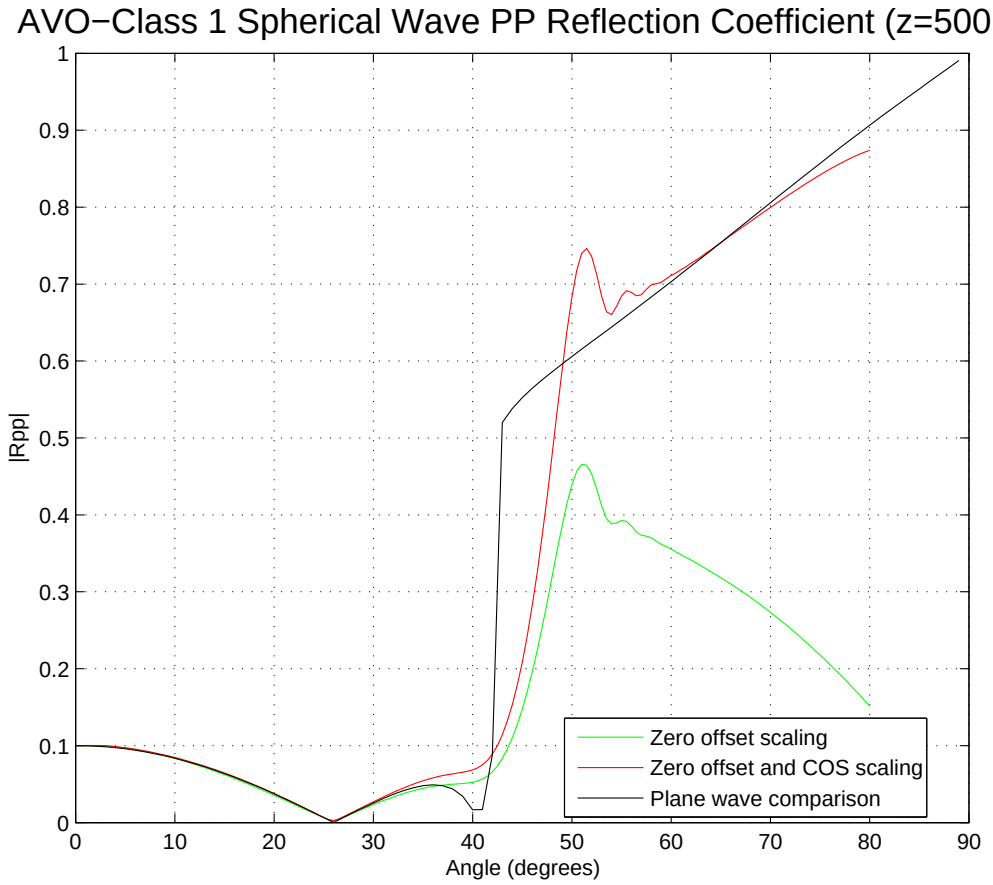

FIG. 9. Scaling comparisons for Class 1 PP-AVO at 500 m. These two scaling methods may be compared with the unit reflectivity method used for the red line in Figure 1a.

(including a phase rotation near the critical angle).

Results of AVO-Class 3 modeling are very different when compared to Class 1. Table 1 shows a P-wave velocity inversion; only S-wave velocities increase across the interface. There is no head wave (and no phase rotation) because there is no critical angle for incident P-waves. Another interesting observation is the apparent lack of depth dependence. The reasons for this apparent depth independence of Class 3 spherical wave AVO-responses are firstly the normalization and secondly the equal angle displays. Away from the critical angle the Class 1 response is also increasingly independent of depth. Class 3 $R_{\rm PP}$ (Figure 4a) always has negative polarity and is nonzero for any angle. Class 3 $R_{\rm PS}$ in Figure 4b begins with zero amplitude and develops negative polarity, as before in Figure 3b. By contrast to Class 1, it passes through zero at about 60° of angle and turns positive. Similar to Class 1 $R_{\rm PS}$, reflection strength returns to zero when approaching 90°. There is no departure from a plane wave comparison for either $R_{\rm PP}$ or $R_{\rm PS}$.

Return path differences are to be expected when anelasticity is introduced in the form of finite Q-factors. The smaller the Q-factors, the larger the attenuation. The return path for converted waves is governed by $Q_{\rm S1}$, which is smaller then $Q_{\rm P1}$ (see Table 2). Consequently, Class 1 spherical PS-wave AVO is more sensitive to decreasing Q-factors than its Class 1 PP-wave comparison. Return path attenuation is compensated for when unit R normalization is employed. Q-factor dependence is reduced for this normalization scheme, as is shown by the Class 1 examples in Figures 5a and 5b. However, converted spherical waves still seem more sensitive to increasing attenuation when compared to spherical P-waves in these examples.

Normalized Q-dependence for spherical wave AVO Class 1, as shown in Figures 5, to some degree mimics normalized depth dependence of the elastic situation (see Figure 1). Increasing Q-factors and increasing depths move normalized spherical wave AVO closer to plane wave comparisons.

There is no Q-factor dependence following normalization of Class 3 spherical PP-wave AVO-responses (Figure 6a). The normalized Class 3 converted wave counterpart in Figure 6b shows some departure for $Q_{\rm P1}$ = 100 (the highest attenuation value considered). Note the different plotting scale for the vertical axes of Figure 6b.

All trace plots in Figures 7 and 8 show phase rotations when compared to the elastic situation. Note that these trace examples are all computed for a depth level of 500 m and $Q_{\rm P1}$ = 100 for attenuation. Amplitude clipping is indicated by colour change: black peaks change to blue, and red troughs change to green when clipped. Also noticeable in these trace plots is the increased pulse width of anelastic converted wave reflections. This wavelet stretch is indicative of a spectral band narrowed by predominant attenuation of higher frequencies.

CONCLUSIONS

Accurate spherical-wave $R_{\rm PP}^{\rm sph}$ and $R_{\rm PS}^{\rm sph}$ reflection coefficients may be calculated numerically by integration over the plane wave coefficients, $R_{\rm PP}^{\rm pw}$ and $R_{\rm PS}^{\rm pw}$. Scaling by similar results obtained using unit reflectivity allows one to identify fundamental deviations from

plane-wave behaviour. Class 1 models show significant amplitude deviations and phase rotations near the critical angle. This is observed even for depths of 2000 m. Class 3 models, which have no P-wave critical angle, show no fundamental deviation from plane-wave behaviour even for depths as shallow as 500 m.

The same method can be modified to calcuate accurate reflection coefficients in the presence of constant Q attenuation. Q-dependence is observed for Class 1, while for Class 3 models, the Q-dependence of $R_{\mathrm{PS}}^{\mathrm{sph}}$ is very weak, and is negligible for $R_{\mathrm{PP}}^{\mathrm{sph}}$.

ACKNOWLEDGEMENTS

The authors wish to thank Professor E. Krebes for helpful discussions related to the theory. Support from CREWES and its industrial sponsorship is gratefully acknowledged.

REFERENCES

Aki, K., and Richards, P. G., 1980, Quantitative seismology, Theory and Methods: Volume 1: W. H. Freeman and Company.

Carcione, J. M., Helle, H. B., and Zhao, T., 1998, Effects of attenuation and anisotropy on reflection amplitude versus offset: Geophysics, **63**, No. 05, 1652–1658.

Downton, J., and Lines, L., 2001, Constrained three parameter AVO inversion and uncertainty analysis, *in* 71st Ann. Internat. Mtg, Soc. of Expl. Geophys., 251–254.

Downton, J. E., and Ursenbach, C., 2006, Linearized amplitude variation with offset (AVO) inversion with supercritical angles: Geophysics, **71**, No. 05, E49–E55.

Hron, F., May, B. T., Covey, J. D., and Daley, P. F., 1986, Synthetic seismic sections for acoustic elastic anisotropic and vertically inhomogeneous layered media: Geophysics, **51**, No. 03, 710–735.

Kjartansson, E., 1979, Constant Q, wave propagation and attenuation: Journal of Geophysical Research, **84**, 4737–4748.

Krail, P. M., and Brysk, H., 1983, Reflection of spherical seismic waves in elastic layered media: Geophysics, **48**, No. 06, 655–664.

Ostrander, W. J., 1984, Plane-wave reflection coefficients for gas sands at nonnormal angles-of-incidence: Geophysics, **49**, No. 10, 1637–1648.

Rutherford, S. R., and Williams, R. H., 1989, Amplitude-versus-offset variations in gas sands: Geophysics, **54**, No. 06, 680–688.

Udias, A., 1999, Principles of Seismology: Cambridge University Press.

Ursenbach, C., Haase, A. B., and Downton, J. E., 2006, Improved modeling of spherical-wave AVO: CREWES Research Report, **18**.

Waters, K. H., 1978, Reflection Seismology: Cambridge University Press.

Weyl, H., 1919, Ausbreitung elektromagnetischer wellen ueber einem ebenen leiter: Ann. Physik, **60**, 481–500.

Winterstein, D. F., and Hanten, J. B., 1985, Supercritical reflections observed in P-wave and S-wave data: Geophysics, **50**, No. 02, 185–195.